CHARACTERIZATION OF RUBBER ISOLATOR NONLINEARITIES IN THE CONTEXT OF SINGLE- AND MULTI-DEGREE-OF-FREEDOM EXPERIMENTAL SYSTEMS

C. M. RICHARDS[†] AND R. SINGH

*Acoustics and Dynamics Laboratory, Department of Mechanical Engineering,
The Ohio State University, Columbus, OH 43210-1107, U.S.A.*

Key non-linear stiffness characterization issues of rubber isolators are clarified, and a process is proposed that includes experiments in single- and multi-degree-of-freedom configurations while different types of excitations are applied. Consequently, important characteristics, via experimental and analytical studies of three isolators, emerge that might not have been revealed in traditional non-resonant testing methods. First, static stiffness experiments are conducted to measure time-invariant load–deflection curves and influences from rubber durometer, isolator geometry and non-linear behavior on the dynamic-to-static stiffness ratio are illustrated. Next, dynamic excitations under random, frequency-sweep and fixed-frequency are employed to investigate how the behavior of each isolator is influenced by type of excitation. Also, the non-linear dynamic stiffness of each isolator is quantified in both single- and multi-degree-of-freedom configurations. Effects of isolator non-linearities on the effective vibration modes of the multi-degree-of-freedom (m.d.o.f.) experimental configuration are shown to be distributed differently for each isolator, yet some correlation is found with the single-degree-of-freedom (s.d.o.f.) experiment. For analytical characterization, the continuous system theory is used to develop a quasi-linear representation of the m.d.o.f. experimental configuration. Isolator dynamic properties determined from the s.d.o.f. experiment are used in this model. Finally, a discrete non-linear model consisting of a non-linear elastic force term is constructed. After execution of a procedure based upon numerical simulation, optimum parameters for this model are found. The characterization studies conducted here form an essential first step for the identification techniques that are improved by *a priori* knowledge of the types of non-linearities present.

© 2001 Academic Press

1. INTRODUCTION

1.1. MOTIVATION AND SCOPE

Understanding the dynamic properties of rubber isolators is necessary for the vibration analysis and optimization of many resilient mounting systems. Consider the generic system of Figure 1(a) where a rigid mass is isolated from a flexible supporting structure. Optimum isolation of the externally excited lumped mass from the supporting structure may be achieved by choosing an elastomer based on the knowledge of its static and dynamic characteristics determined from laboratory experiments. The resulting static stiffness data

[†]Present address: Department of Mechanical Engineering, The University of Louisville, Louisville, KY 40292, U.S.A.
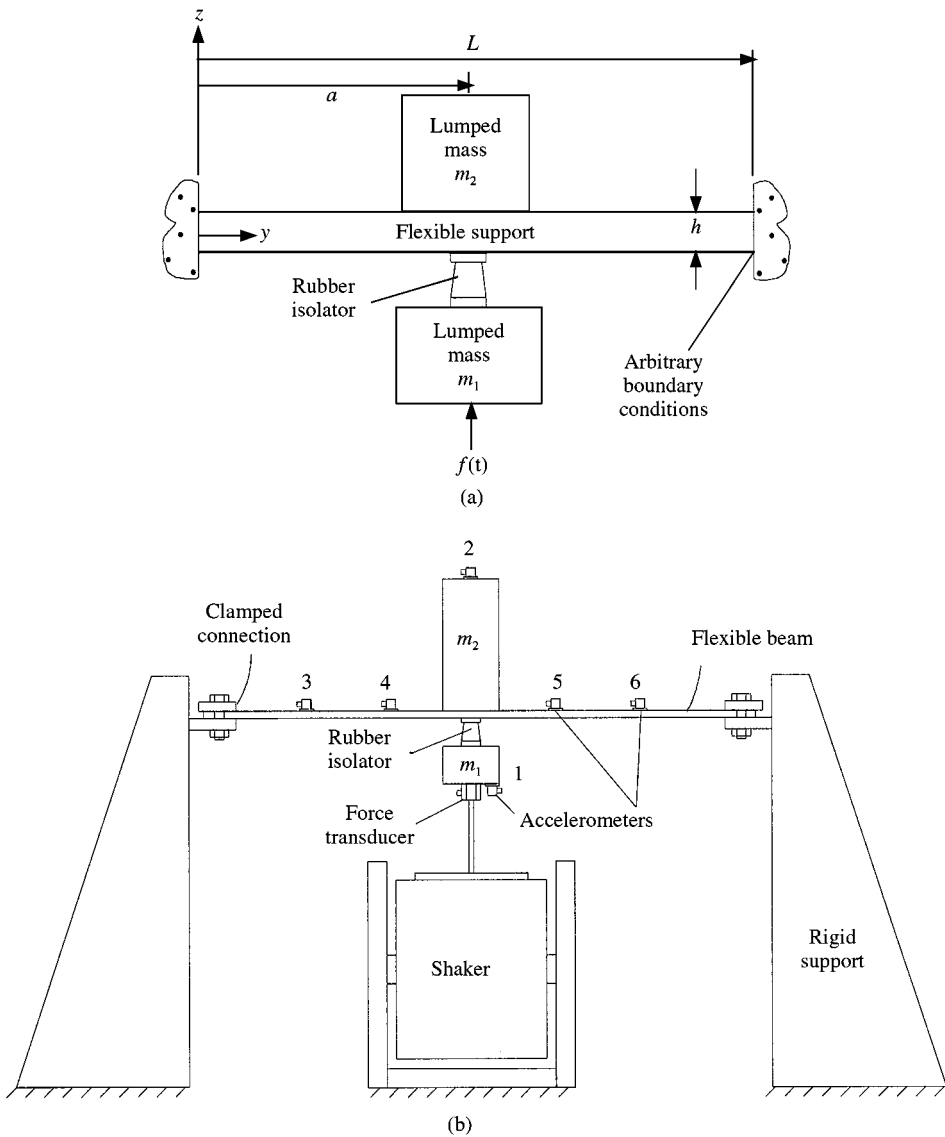
© 2001 Academic Press

Figure 1. Problem formulation via an m.d.o.f. vibration system with a non-linear elastomeric isolator: (a) conceptual system; (b) experimental implementation.

may be useful for mean load requirements, but inevitably, dynamic stiffness differs from that measured from static tests [1], though some limited trends have been found relating static-to-dynamic stiffness through durometer [1, 2]. Therefore, as a part of traditional industrial design practice, non-resonant dynamic stiffness type experiments are often carried out to determine viscoelastic properties where sinusoidal displacement excitation is applied in single or multiple directions and transmitted forces are measured to determine the complex stiffness at fixed frequencies with given amplitudes [3,4]. From these experiments, the inherent non-linear behavior of rubber isolators is often apparent under finite motions [1, 5–7]. Therefore, it is necessary to extend the experimental and analytical capability beyond the linear assumptions [3, 8–11] to capture the amplitude-dependent non-linear behavior of rubber isolators.

The mathematical analysis of non-linear isolators is insightful for both design and performance purposes [12–15]. However, it is often challenging to determine an explicit model of the non-linear elastic and dissipative behavior of physical isolators so that such analysis can be conducted. Therefore, for physical isolators of unknown nonlinear behavior, model identification is necessary in order to determine an accurate representation of the isolator. Then, analytical techniques using the identified model as the basis for the analysis could be utilized. Unfortunately, many model identification methods for non-linear systems have their limitations [16] since knowledge of the underlying mathematical form for best describing the dynamic behavior is often helpful to aid in the identification process. Therefore, experimental characterization that reveals non-linear behavior should be employed as a first step to better understand rubber isolator dynamics under different static and dynamic loading conditions. From this understanding, a select mathematical form may be realized for use in the identification techniques [16, 17].

In this article, experimental and analytical characterization is applied to model three different rubber isolators. Unlike much of the research conducted in the past [18–23], each isolator is modelled as part of a multi-degree-of-freedom (m.d.o.f.) configuration. Both component (single-degree-of-freedom (s.d.o.f.) configuration) and system (m.d.o.f. configuration) type experiments are first performed to address the following key issues related to isolator performance and isolation system design: (1) What are the influences of rubber durometer, isolator geometry and non-linear stiffness on the effective dynamic-to-static stiffness ratio? (2) Do the types of excitations experienced by the isolators influence their non-linear behavior? (3) How do isolator non-linear stiffness characteristics determined from s.d.o.f. experiments influence m.d.o.f. dynamics and do relations exist between the two configurations? (4) Are isolator properties determined from s.d.o.f. experimental configuration valid for modelling isolator behavior under m.d.o.f. configuration? (5) Can non-linear m.d.o.f. models be constructed to accurately describe the non-linear elastic behavior of rubber isolators in m.d.o.f. configuration? The first three issues are addressed by direct analysis of the measured data from the s.d.o.f. and m.d.o.f. experimental configurations. However, the last two issues must be determined from m.d.o.f. system modelling. Therefore, two different m.d.o.f. system models are constructed, a continuous quasi-linear and a discrete non-linear system model. The dynamic characteristics predicted from these models are then compared with experiment. The knowledge gained from this study will be utilized in a future article investigating the use of non-linear system identification [16, 17] of the three rubber isolators.

1.2. RESEARCH ISSUES

In addition to the traditional non-resonant method [3, 4], other methods for characterizing rubber isolators have also been developed [24, 8–11]. An indirect method has been developed where the rubber isolator specimen is placed between two rigid masses [24]. From the measured responses of the masses (measurement of the applied forces is unnecessary), the dynamic stiffness of the isolator is determined through approximations based on the measured spectra. Since the masses are unconstrained, rotational and lateral stiffness may also be measured, although the method is limited to higher frequency ranges due to assumptions made on the response frequency with respect to the system natural frequencies. Another experimental method has also been developed for determining the high-frequency dynamic properties of rubber isolators [8], and a model based on statistical energy analysis (SEA) has been realized for describing the high-frequency dynamic behavior. Also in the mid- and high-frequency range, the transfer matrix approach has been

utilized to predict the vibration attenuation of airplane stowage bin isolators under (s.d.o.f.) test configuration [9]. Automotive engine mounts have been modelled using SEA where the radiation and structural coupling losses are derived so that the mount model can be utilized in a SEA system model [10]. Also, power flow analysis has been investigated for machine isolators in an (m.d.o.f.) configuration where the flexibility of the supporting structure is considered [11].

Although, the experimental methods discussed in the aforementioned literature determine the frequency-dependent behavior of rubber isolators [3, 4, 8, 24], the modelling approaches are linear [3, 8–11]. However, rubber isolators are inherently non-linear in nature and this behavior is apparent under finite motions [1, 5–7]. In addition, material composition, static pre-load and mount geometry can influence the non-linear behavior [1, 5–7]. As a result, analytical studies have been undertaken to address the non-linear dynamic behavior of rubber isolators [12–15]. For example, studies have investigated the dependence of transmissibility performance indices (i.e., maximum amplitude and frequency of transmissibility, resonance and non-resonance critical frequency, jump width and high-frequency attenuation rate) on the non-linear parameters of isolators in s.d.o.f. configuration [12]. The study was conducted for isolators with symmetric and asymmetric non-linear damping and stiffness. Also, isolators of given non-linear forms have been examined under different shock excitations where a perturbation method was used to determine closed-form solutions [13]. Non-linear damping showed relevant influence on the s.d.o.f. response characteristics and improved response from a non-linear damping model with a negative coefficient was reported.

An additional analysis has been conducted to investigate transient performance of isolator and vibration absorber configurations [14]. Non-linear cubic damping was assumed for describing isolator non-linear dissipative behavior, though Coulomb damping was also assumed for one configuration. For the analysis of isolators under random excitations, a method has been developed to determine response parameters such as peak displacement and root-mean-square (r.m.s.) acceleration of the isolated mass [15]. These response parameters were investigated as a function of strength of the isolator non-linearity, which was described as a cubic hard spring, cubic soft spring or tangent spring (i.e., elastic force described by the tangent function).

For the development of analytical models of non-linear isolators based on experimental data, s.d.o.f. methods have been investigated [18–23]. Single d.o.f. models have been examined to describe the non-linear stiffness and damping characteristics where two different approaches were discussed, one for modelling the hysteresis loops and another for modelling the transmissibility functions [18]. Also, an alternating time–frequency identification technique has been developed [19] based on the Bouc–Wen model [20]. The technique has been shown to be relatively insensitive to measurement noise for both force and displacement controlled tests and was utilized to identify a wire-cable isolator. Another non-linear rubber model has been developed by decomposing the transmitted force into elastic, friction and viscous components [21]. From this model, a procedure was then developed for extracting the parameters from measured hysteresis loops. Models with alternate spring, damper and mass arrangements have been considered to represent the viscoelastic behavior of a mount [22]. A successful model was determined by examining the measured frequency response characteristics of an experimental system made up of a rigid mass and the isolation mount. Finally, temporal and spectral system identification methods have been utilized to identify a non-linear rubber isolator in s.d.o.f. configuration [23]. Non-integer exponent-type models were found to be particularly successful at describing the non-linear elastic force of the isolator. Nevertheless, additional research is necessary in order to improve this model.

2. PROBLEM FORMULATION

To establish the m.d.o.f. context, consider the system shown in Figure 1(a) where a rigid mass m_1 is mounted to a flexible beam from the bottom at $y = $ a via a rubber isolator. A second lumped mass m_2 is also rigidly connected to the top of the beam at $y = a$. This generalized arrangement could represent a variety of practical systems, e.g., an engine or gearbox isolated from the chassis of an automobile or the fuselage of an aircraft. For experimental studies, the system in Figure 1(b) is constructed and analyzed first using the linear system theory. The flexible beam is described by the Euler's beam equation [25]. Due to shear force loading from the isolator, the dynamics of the beam must be given by two separate equations. These equations along with the equation of motion of m_1 are

$$\frac{\partial^2}{\partial y^2}\left[EI(y)\frac{\partial^2 u_j(y, t)}{\partial y^2}\right] = -\rho'(y)\frac{\partial^2 u_j(y, t)}{\partial t^2}; \quad \begin{matrix} j = 1, \ 0 \leqslant y \leqslant a, \\ j = 2, \ a \leqslant y \leqslant L, \end{matrix}$$

$$m_1\ddot{x}_1(t) + k_d(x_1(t) - u_j(a, t)) = 0, \tag{1a, b}$$

where E is the elastic modulus of the homogeneous beam, $I(y)$ is the cross-sectional area moment of inertia about the x-axis (perpendicular to the plane shown), $\rho'(y)$ is the mass per unit length, $u_j(y, t)$ is the transverse displacement of the beam, $x_1(t)$ is the displacement of m_1, and k_d is the effective linear dynamic stiffness coefficient of the isolator. Also refer to Appendix A for a list of symbols. The harmonic solution, $u_j(y, t) = \phi_j(y)e^{i\omega t}$ and $x_1(y, t) = \Phi e^{i\omega t}$, assumption results in the eigenvalue problem

$$\frac{\partial^2}{\partial y^2}\left[EI(y)\frac{\partial^2 \phi_j(y)}{\partial y^2}\right] - \omega^2\rho'(y)\,\phi_j(y) = 0; \quad \begin{matrix} j = 1, \ 0 \leqslant y \leqslant a, \\ j = 2, \ a \leqslant y \leqslant L, \end{matrix}$$

$$-\omega^2 m_1\Phi + k_d(\Phi - \phi_j(a)) = 0, \tag{2a, b}$$

which is solved after applying the appropriate boundary conditions at $y = 0$ and L and satisfying continuity, slope, force and moment loading conditions at $y = a$.

The chief objectives of this study are to experimentally and analytically characterize three rubber isolators when each is subjected to static time-invariant and dynamic (random, swept-sine and fixed-sine) force excitations in both s.d.o.f. and m.d.o.f. configurations. The characterization study begins by performing static experiments to determine the time-invariant stiffness of each isolator. Then dynamic s.d.o.f. system experiments are performed to determine effective (linearized) damping and stiffness properties of the isolators. Next, the isolators are placed in the m.d.o.f. experimental system of Figure 1(b) and experiments are performed to characterize the rubber isolators under m.d.o.f. configuration. Equation (1a, b) is used to describe the linearized system response of the m.d.o.f. experimental system in the 0–128 Hz frequency range. Finally, non-linear models are constructed to describe the behavior of the isolators under m.d.o.f. configuration and numerical simulation is used to predict the non-linear responses that are then compared with experimental data.

3. STATIC BEHAVIOR

Each isolator is first subjected to the static experiment of Figure 2(a) where static loads f_s are applied in both tension and compression by adding known masses to the weight containers. After a period of $t_r = 10$ s, the static displacement x_s of the isolator is recorded from the dial indicator. The recording time t_r was held constant for all three isolators during
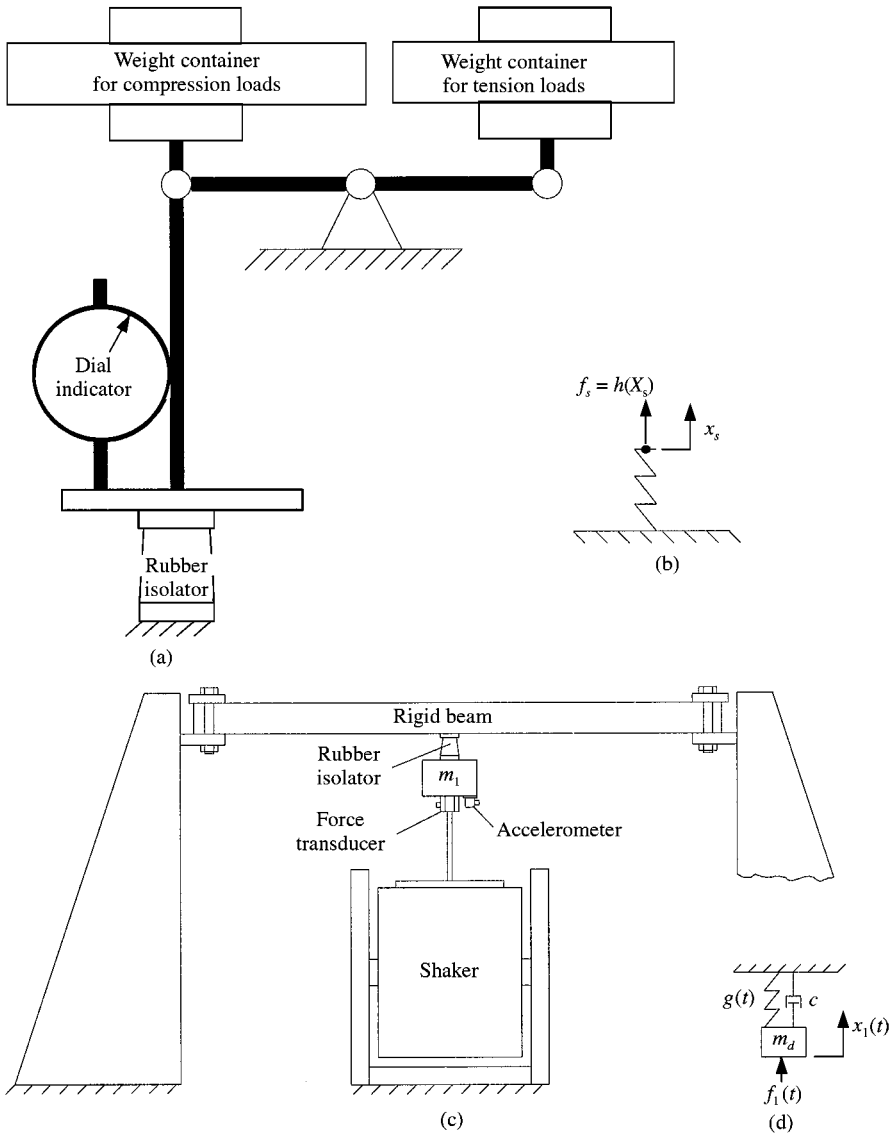
Figure 2. Isolator characterization experiments: (a) static stiffness test; (b) static stiffness model; (c) single-degree-of-freedom dynamic test; (d) single-degree-of-freedom dynamic model.

every weight application for comparative purposes. Choice of t_r is based on observations of how long it requires initial "fast responding" displacement of the isolator to occur. The free end of the isolator continues to displace after this period; however, the response is much slower, indicative of creep. Although not reported, additional tests were conducted with longer recording times, resulting in static stiffness curves with slightly more hysteresis. However, the general shapes of the curves remained the same.

The analytical model that is valid for this experiment is shown in Figure 2(b) where the function $h(x_s)$ may be non-linear. Illustrated in Figures 3–5 are the rubber isolators considered in this study. Isolator 1 of Figure 3(a) is composed of a solid tapered cylinder made from neoprene rubber with 2 aluminum-mounting plates fastened to each end. The
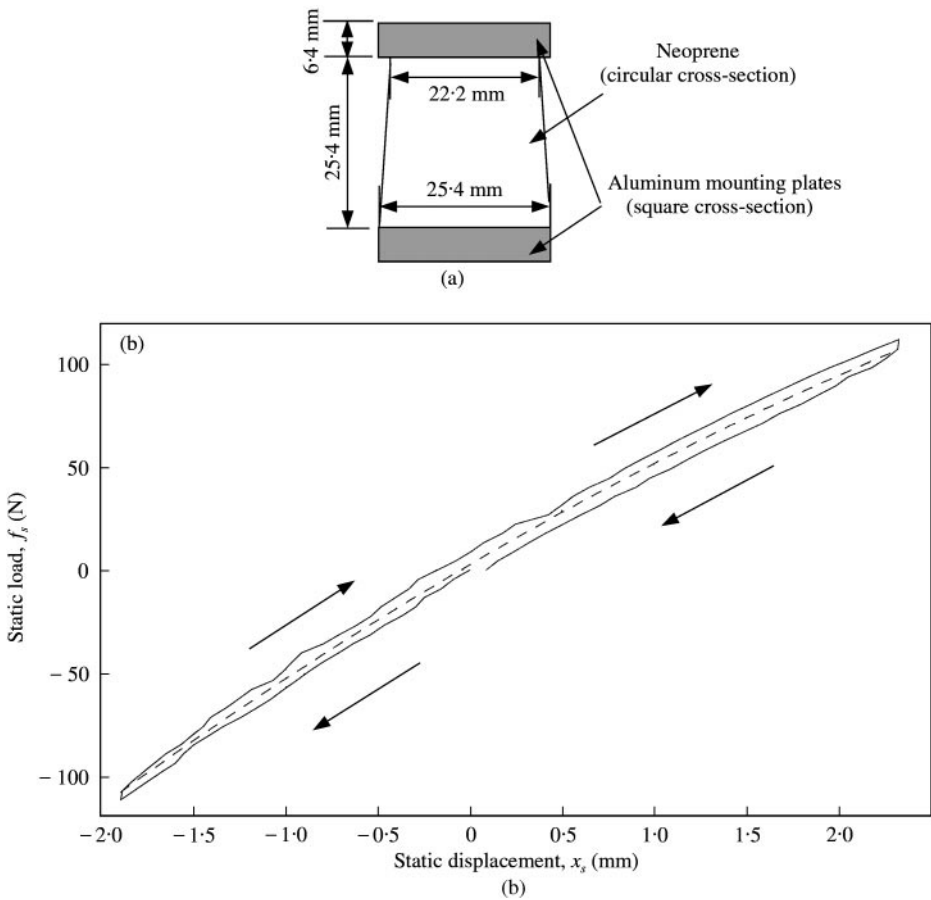
Figure 3. Isolator 1: (a) schematic of isolator; (b) measured static stiffness results. Arrows indicate history of the applied static load. ——, Measured; – – – – –, model $\Xi_{0,2}$.

neoprene has a Shore A hardness (durometer) of 45. Figure 3(b) illustrates this isolator's stiffness curve where the arrows indicate the history of the applied static load, i.e., first compression loads are applied, and then released. Next, tension loads are applied, and then released. Notice the presence of hysteresis from the open-looped curve. Also, notice a slight softening in stiffness when in tension and a slight hardening in stiffness when in compression. Isolator 2 of Figure 4(a) is composed of a rubber block made from natural rubber with a 35 durometer. Two square aluminum-mounting plates are bonded to the ends of the rubber block. Figure 4(b) illustrates the resulting stiffness curve where hysteresis is again apparent although the stiffness appears linear. Finally, Isolator 3 of Figure 5(a) is a neoprene (30 durometer) bubble-type isolator with a hollow cavity. Figure 5(b) illustrates the stiffness curve that matches the specifications provided by the manufacturer [26]. In addition to hysteresis, the compression segment of the static stiffness curve exhibits a significant amount of non-linearity when compared with the tension segment. It is believed that the initial softening stiffness is due to the collapsing of the isolator. Then, once in a collapsed state, hardening stiffness results from compression of the isolator's walls against one another. This type of non-linear characteristic caused by mount geometry has also been reported by Harris [6].
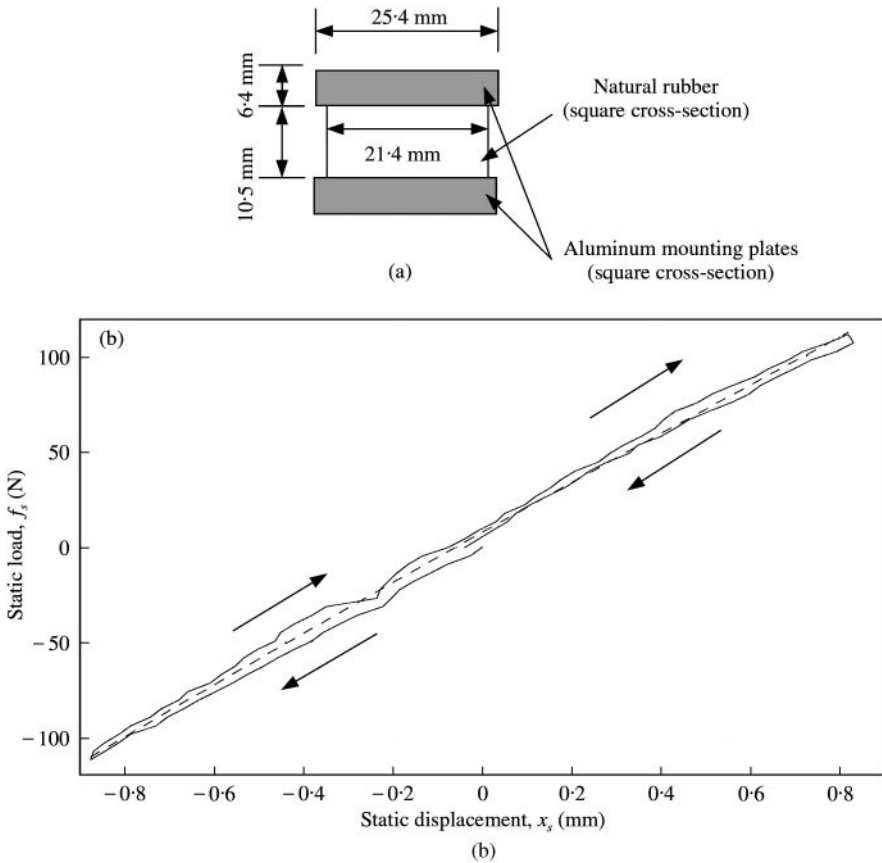
Figure 4. Isolator 2: (a) schematic of isolator; (b) measured static stiffness results. Arrows indicate history of the applied static load. ——, Measured; – – – –, model $\Xi_{0,2}$.

The static stiffness data presented here are the type of data often provided in product catalogs or even listed in machinery specifications [15]. However, it is uncertain whether such data can lead to the dynamic elastic force $g(x(t))$. To quantify the static characteristics, polynomials of the following form are fit to the static data using polynomial regression [27]:

$$\Xi_{a,b}(x_s) = \sum_{j=a}^{b} k_j x_s^j. \tag{3}$$

Model $a = 0$ is an unphysical representation of an isolator since zero static displacement ($x_s = 0$) results in a non-zero static force ($\Xi_{0,b}(0) = k_0 \neq 0$). However, the presence of hysteresis results in a bias in the static data. This causes "bowing", in the positive force or tension direction, of the curve-fit of the equations $\Xi_{1,b}(x_s)$ that do not contain the constant term k_0, since these equations must pass through the origin. To alleviate "bowing", $\Xi_{0,b}(x_s)$ models that do not have to pass through the origin are considered, keeping in mind that the constant term must be ignored when utilized for physical representation.

Often, accuracy of polynomial regression is determined from the coefficient of determination [27], which indicates the amount of uncertainty from the mean that is explained by the model. However, the static data of the isolators deviate about a slope. Therefore, the coefficient of determination is redefined for this study to indicate the amount
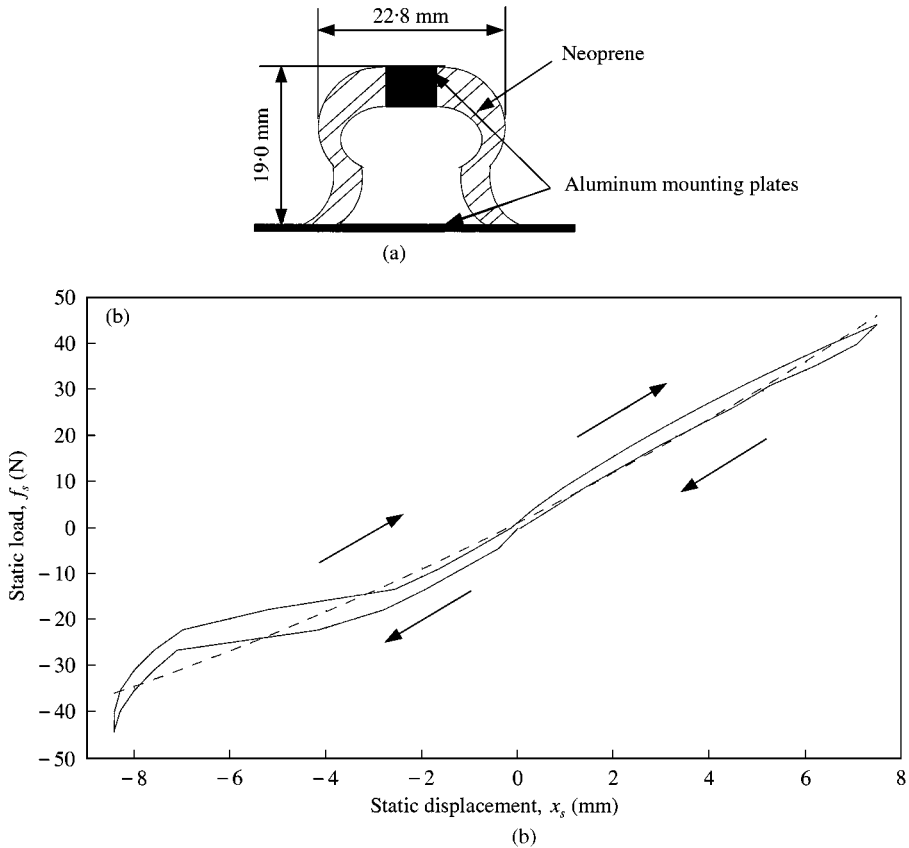
Figure 5. Isolator 3: (a) schematic of isolator; (b) measured static stiffness results. Arrows indicate history of the applied static load. ——, Measured; – – – – –, model $\Xi_{0,2}$.

of uncertainty explained by the model, where the uncertainty is measured from a line fit to the data which pass through the origin, i.e., $\Xi_{1,1}(x_s)$. This new coefficient of determination is given as

$$R^2_{a,b} = \frac{S_{1,1} - S_{a,b}}{S_{1,1}}, \quad S_{a,b} = \sum_{i=1}^{n} (f_{si} - \Xi_{a,b}(x_{si}))^2, \tag{4a, b}$$

where n is the number of data points collected from the static experiment. Table 1 lists results for linear ($b = 1$), quadratic ($b = 2$) and cubic ($b = 3$) equations with and without constant terms, i.e., $a = 0$ or 1, respectively. For Isolator 1, less than 10% improvement is gained with the inclusion of the constant term, i.e., the $\Xi_{0,b}(x_s)$ models compared with $\Xi_{1,b}(x_s)$ models. However, for Isolator 2 the constant term significantly improves the models where $R^2_{0,b} > 70\%$ and $R^2_{1,b} < 30\%$. With the exception of $\Xi_{0,1}(x_s)$ compared with $\Xi_{1,1}(x_s)$, the constant term improves the model by less than 3% for Isolator 3. For Isolators 1 and 3, quadratic models $\Xi_{a,2}(x_s)$ better fit the data over linear models $\Xi_{a,1}(x_s)$; however, inclusion of cubic terms, i.e. $\Xi_{a,3}(x_s)$, yields little improvement. No significant improvement is obtained with the inclusion of quadratic or cubic terms for Isolator 2 indicating that the static stiffness for this isolator is close to linear.

TABLE 1

Least-squares estimates of static stiffness curves, corresponding to equation (3)

Model	Parameter	Isolator		
		1	2	3
$\Xi_{1,1}(x_s)$	k_1 (kN/m)	50·9	129·5	4·9
	$R^2_{1,1}$ (%)	0·0	0·0	0·0
	k_0 (N)	−2·2	6·9	3·6
$\Xi_{0,1}(x_s)$	k_1 (kN/m)	51·0	131·0	5·0
	$R^2_{0,1}$ (%)	9·7	70·5	42·8
	k_1 (kN/m)	51·7	131·3	5·3
$\Xi_{1,2}(x_s)$	k_2 (MN/m^2)	−2·2	13·5	0·1
	$R^2_{1,2}$ (%)	42·9	28·5	57·7
	k_0 (N)	2·7	7·8	1·2
$\Xi_{0,2}(x_s)$	k_1 (kN/m)	52·0	130·6	5·3
	k_2(MN/m^2)	−3·2	−4·0	0·1
	$R^2_{0,2}$ (%)	49·7	71·6	59·9
	k_1 (kN/m)	51·2	134·7	5·6
$\Xi_{1,3}(x_s)$	k_2 (MN/m^2)	−2·3	13·0	0·1
	k_3(MN/m^3)	203·6	−7516·1	−5·9
	$R^2_{1,3}$ (%)	43·1	29·3	58·4
	k_0 (N)	2·9	8·0	1·2
	k_1 (kN/m)	50·8	136·2	5·5
$\Xi_{0,3}(x_s)$	k_2(MN/m^2)	−3·4	−5·2	0·1
	k_3(MN/m^3)	428·4	−12600·0	−6·0
	$R^2_{0,3}$ (%)	50·6	73·9	60·7

The $\Xi_{0,2}(x_s)$ models are plotted over the respective static stiffness data for each isolator in Figures 3(b), 4(b) and 5(b). For Isolators 1 and 2, visual comparison validates the goodness-of-fit. However, for Isolator 3 the fit does not accurately represent the data. A higher order polynomial would be necessary in order to more accurately describe the multiple changes in slope on the compression portion of the static stiffness curve. Although not illustrated, it should be noted that cubic models compare well with the quadratic models illustrated. In addition, for Isolator 2, linear, quadratic and cubic models compare closely. These models will be revisited using the preceding analysis.

4. DYNAMIC BEHAVIOR BASED ON s.d.o.f. EXPERIMENTS

The s.d.o.f. dynamic experiment is illustrated in Figure 2(c) where a cylindrical block m_1 is isolated from the center of a steel beam via one of the isolators. The beam, whose ends are clamped to massive supports, has the following dimensions: unconstrained length $L = 540$ mm, width $w = 100$ mm and thickness $b = 25.40$ mm. The first beam natural frequency is 468 Hz, which is more than 3 times the greatest frequency of interest ($f_{max} = 128$ Hz). Therefore, the s.d.o.f. model depicted in Figure 2(d) is valid. The dynamic force of each isolator in the normal direction is defined as $G(\Delta \dot{x}(t), \Delta x(t))$, where $\Delta \dot{x}(t)$ and $\Delta x(t)$ are the relative velocity and displacement across the isolator, respectively. Since the beam is assumed rigid, $\Delta \dot{x}(t) = \dot{x}_1(t)$ and $\Delta x(t) = x_1(t)$. Also, assuming linear viscous

damping of coefficient c, G is rewritten as $G(\dot{x}_1(t), x_1(t)) = c\dot{x}_1(t) + g(x_1(t))$ where $g(x_1(t))$ is the non-linear dynamic elastic force of the isolator. Experimental characterization of each isolator under this configuration involves measurement of acceleration $\ddot{x}_1(t)$ of m_1 with a piezoelectric accelerometer and measurement of excitation $f_1(t)$ applied to m_1 by an electrodynamic shaker with a piezoelectric force transducer. Before each isolator is tested, a "break-in" period is initially conducted where m_1 is subjected to random excitation up to 100 Hz at five excitation levels for 60 s.

Isolator behavior is first examined under random excitation applied to m_1 at 5 r.m.s. levels. The random excitation is white noise evenly distributed over the frequency range (0–1024 Hz). Excitation and response signals are sampled at 2048 Hz for 192 s (24 blocks of 2^{14} data points). Since the Nyquist frequency ($f_N = 1024$ Hz) is much greater than the highest frequency of interest ($f_{max} = 128$ Hz), an eighth-order Chebyshev type I digital low-pass filter with a cut-off frequency at 100 Hz is applied to the data. The data are then decimated by 8 resulting in $f_{max} = 128$ Hz. Accelerance spectra are then calculated using the "H_1" frequency response estimator [28, 29] where 48 averages are taken using a Hanning window to reduce leakage error. Figure 6 illustrates accelerance functions $H_{11}(\omega) \approx \ddot{X}_1(\omega)/F_1(\omega)$ for the three isolators where the first subscript indicates the response location and the second subscript indicates the excitation location. Although this nomenclature is unnecessary for s.d.o.f. analysis, it will be useful for the m.d.o.f. analysis to follow. Only accelerance spectra resulting from the maximum and minimum excitation levels are illustrated. The accelerance spectra resulting from intermediate levels of excitation lie somewhere between these two curves. The accelerance spectra are used in a modal analysis software [30] to determine effective natural frequencies and effective damping
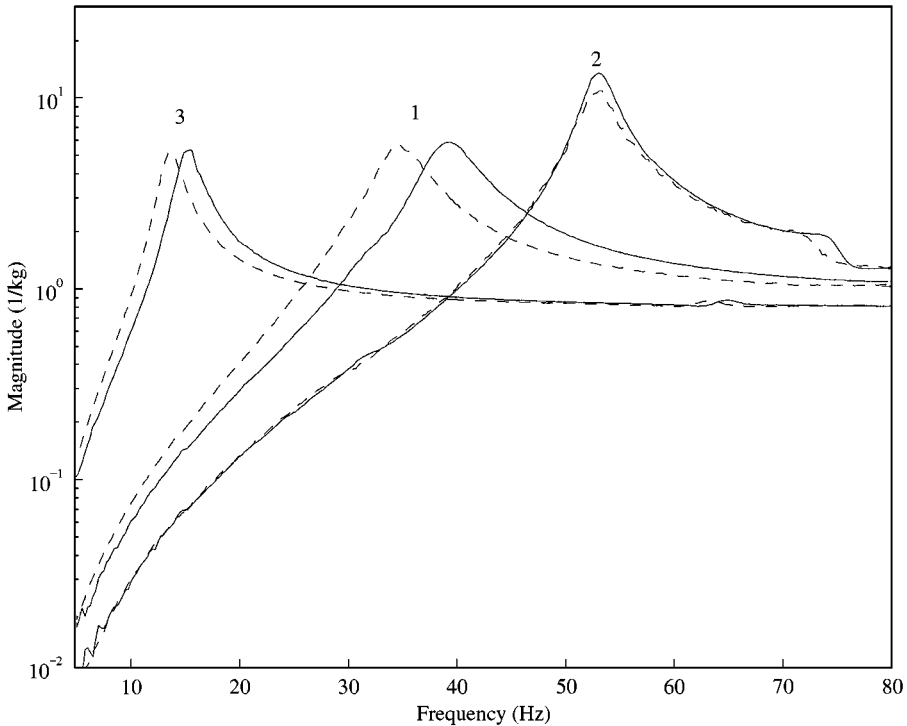

Figure 6. Magnitude of measured accelerance spectra from s.d.o.f. configuration under random excitation. Numbers indicate isolator used in s.d.o.f. configuration. ———, lowest force level, – – – – –, highest force level.

TABLE 2

Effective modal and physical properties of isolators under s.d.o.f. configuration, given $m_d = 1.3$ kg

Isolator	$|f(t)|_{r.m.s.}$ (mN)	Effective modal parameters				Effective physical properties		
		f_n (Hz)	Δf_n (Hz)	ζ (%)	$\Delta\zeta$ (%)	k_d (kN/m)	β	c (N s/m)
	12·8	39·3	0·0	6·8	0·0	81·0	1·6	7·1
	86·2	38·0	−1·3	7·2	0·4	75·9	1·5	7·2
1	157·7	37·4	−1·9	7·3	0·5	73·3	1·4	7·3
	293·7	36·6	−2·7	7·3	0·5	70·3	1·4	7·1
	884·2	34·8	−4·5	7·1	0·3	63·5	1·2	6·6
	13·1	53·2	0·0	2·9	0·0	148·7	1·1	4·1
	89·3	53·0	−0·2	3·0	0·1	147·6	1·1	4·3
2	164·3	53·0	−0·2	3·0	0·1	147·5	1·1	4·3
	305·8	53·0	−0·2	3·1	0·1	147·5	1·1	4·3
	915·2	52·9	−0·3	3·3	0·3	147·1	1·1	4·6
	15·2	15·3	0·0	6·9	0·0	12·3	2·5	2·8
	97·9	14·9	−0·4	6·9	0·1	11·7	2·4	2·8
3	180·7	14·7	−0·6	7·2	0·4	11·3	2·3	2·8
	334·3	14·4	−1·0	7·5	0·6	10·9	2·2	2·9
	1003·8	13·7	−1·6	7·6	0·7	9·9	2·0	2·7

ratios for each random excitation level. Results are given in Table 2 where it is seen that all three isolators illustrate a decrease in effective natural frequency as $|f(t)|_{r.m.s.}$ is increased. However, this decrease is much smaller for Isolator 2, indicating relatively linear elastic behavior in contrast to the non-linear elastic behavior of Isolators 1 and 3. This may be a result of a smaller percentage of carbon black in the natural rubber compound that makes up Isolator 2, since the addition of carbon black has been shown to cause the dynamic properties of rubber to be more dependent on the amplitude of the dynamic strain [6]. Also note that for all three isolators, the change in damping ratio as a function of excitation amplitude is small, hence validating the linear viscous damping assumption.

Additional observations can be made about the isolators from the random excitation data by examining the relationship between durometer and the ratio $\beta = k_d/k_s$ where k_d and k_s are effective dynamic and static stiffness, respectively. Harris [1] and Allen *et al.* [2] suggest a linear trend between β and durometer. Before calculating β, the effective dynamic stiffness coefficients k_d at each excitation level must first be determined for each isolator. Since an s.d.o.f. configuration is assumed, k_d can be determined once the contributing dynamic mass m_d is known. The dynamic mass m_d is determined from the mass line of the accelerance functions well beyond the peak frequency, which is possible since the Nyquist frequency is 1024 Hz. For all three isolators, a dynamic mass of $m_d \approx 1.3$ kg is estimated. For this value of m_d, the effective dynamic stiffness coefficients k_d of the three isolators are calculated at each excitation level and listed in Table 2. The static stiffness coefficient k_s is approximated from the linear least-squares curve-fits $\Xi_{1,1}(x)$ of Table 1. The ratios β are now calculated for the 5 r.m.s. levels and are also listed in Table 2. Results are plotted versus durometer in Figure 7. The five data points given for each isolator correspond to each excitation level. Included in this plot are data points of β provided by Harris [1] along with a curve that approximates the trend in the data. Also included are data ranges of β provided by Allen *et al.* [2]. For Isolators 1 and 2, β matches well with what has been reported in the literature. For Isolator 2, the values for β are closely spaced together due to the linear
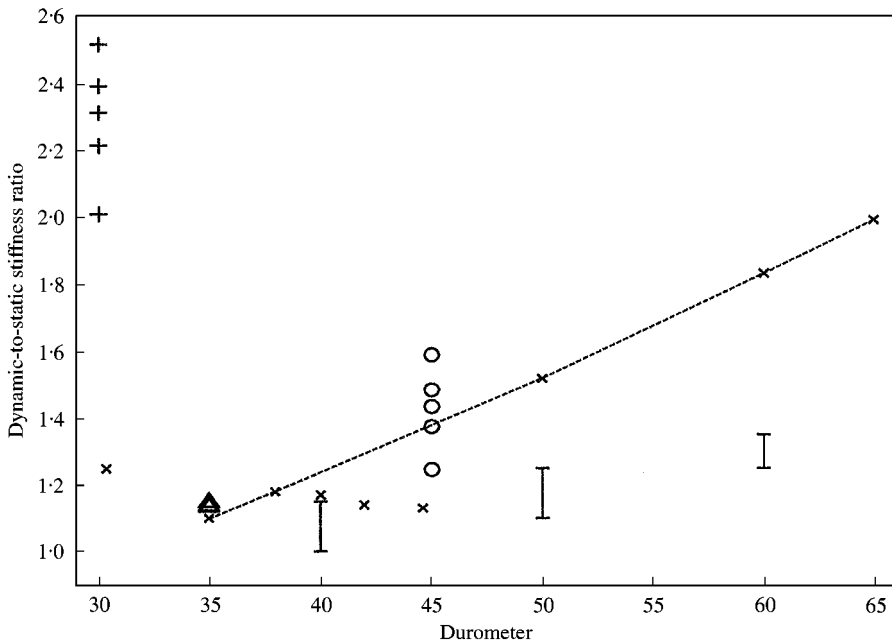
Figure 7. Dynamic-to-static stiffness ratio β as a function of rubber durometer. $\times$, data given by reference [1]; $- - - -$, curve given by reference [1]; I, range given by reference [2]; $\bigcirc$, measured for Isolator 1; $\triangle$, measured for Isolator 2; $+$, measured for Isolator 3.

stiffness behavior of the isolator and hence very little change in the effective dynamic stiffness coefficient k_d. For Isolator 1, the values for β are spread apart since k_d changes with excitation level. This illustrates that although the durometer may indicate trends in β, the non-linear isolator stiffness may present deviations from these trends. For Isolator 3, recall Figure 5(a), which illustrates the more complex cross-section of this isolator compared with Isolators 1 and 2. Consequently, isolator geometry may contribute to why β for Isolator 3 does not agree with the trends provided by the literature. This illustrates that not only rubber nonlinearities but also isolator shape can cause deviations in the relation between β and durometer.

Next, swept-sine excitation with positive and negative sweep rates is applied to m_1 between 5 and 105 Hz in 1 Hz steps. Differences in the accelerance spectra resulting from the positive and negative sweep rates should indicate non-linear behavior. However, for all three isolators, no significant differences in the accelerance functions exist, indicating that the behavior of the isolators is linear under swept-sine excitation. Finally, sinusoidal excitations at fixed frequencies are applied separately to observe sub- or super-harmonic response. Super-harmonics are present in the auto-power spectrum of the acceleration of m_1; however, the harmonics are at least 2 orders of magnitude below the fundamental frequency suggesting that non-linear behavior is not very strong under sinusoidal excitation conditions. The linear behavior of the isolators under swept- and fixed-sine excitations indicates that type of excitation may play a role in how the isolators behave since non-linear behavior was observed under random excitations (note that force levels between all the different excitation types are comparable). This observation is useful for current practitioners who utilize complex stiffness data from sinusoidal excitation tests to characterize isolators and then implement these isolators under real operating conditions where random excitations are prevalent.

5. DYNAMIC BEHAVIOR BASED ON m.d.o.f. EXPERIMENTS

The m.d.o.f. configuration of Figure 1(b) is considered next where the rigid mass m_1 is isolated from an aluminum beam, which differs from the previous steel beam, via one of the rubber isolator specimens. Note that m_1 is the same cylindrical block used in the s.d.o.f. configuration. The aluminum beam, whose ends are clamped to massive supports, has the following dimensions: $L = 670$ mm, $w = 100$ mm and $b = 9.56$ mm. The isolator is located at the center of the beam where a second mass m_2 (6·7 kg) is connected rigidly. As with the s.d.o.f. configuration, a piezoelectric force transducer measures the excitation $f_1(t)$ of m_1 provided by an electrodynamic shaker. However, for this configuration, accelerations $\ddot{x}_i(t)$ at locations i, $i \in [1, 6]$, are measured by piezoelectric accelerometers in order to measure mode shapes. Signal processing used here is equivalent to that used for the s.d.o.f. experiments.

The m.d.o.f. configuration is first investigated under random excitation at 4 r.m.s. levels. Characteristics of the random excitation are similar to that used for the s.d.o.f. experiments. Compliance spectra are estimated as illustrated in Figures 8–10 at the lowest and highest excitation levels. Effective natural frequencies (f_1, f_2), damping ratios (ζ_1, ζ_2) and modes shapes (ϕ_1, ϕ_2) are determined from the compliance functions using the modal analysis software [30] and f_1, f_2, ζ_1, and ζ_2 are given in Table 3 for the first and second peaks along with changes in these values as a function of excitation level. Similar to the s.d.o.f. compliance spectra, the peak frequencies decrease with increasing $|f(t)|_{r.m.s.}$, although this change is again small for Isolator 2. Therefore, it is concluded that Isolator 2 exhibits the least amount of non-linear behavior under random excitation for both s.d.o.f. and m.d.o.f. configurations.

Although not seen in Figures 8–10, the third peak (effective mode 3) occurs at $f_3 = 63.0$ Hz for all three isolators. The frequency of the third peak is independent of which isolator is placed in the m.d.o.f. configuration since the mounting location is at $a = 0.5L$ and this location is a node of the effective mode shape, which is described as second beam bending motion and no relative motion between the isolated mass m_1 and the center of the beam. This is also the reason why this peak does not occur in $H_{11}(\omega)$ or $H_{21}(\omega)$ plotted in Figures 8–10 since the response locations 1 and 2 are at the node of effective mode 2.

There are additional observations to make concerning these data. However, to improve the readability of this discussion, the following nomenclature is introduced. The experiment with Isolator m ($m = [1, 3]$) placed in the m.d.o.f. configuration will be referred to as the m.d.o.f.m experiment. Likewise, each s.d.o.f. experiment of section 4 will be referred to as the s.d.o.f.m experiment for each mth isolator. The first observation concerns the m.d.o.f.1 compliance spectra of Figure 8. Notice that the second peak shifts more than the first peak. To determine why this occurs, the first and second effective mode shapes of the m.d.o.f. configuration are first described. The effective mode shape 1 is composed of first beam bending motion with m_1 in phase with the center of the beam. For effective mode shape 2, m_1 is out of phase with the first beam bending motion. Consequently, one might expect larger relative motion $\Delta x_{12}(t) = x_1(t) - x_2(t)$ to occur across the isolator for the second mode compared with the first mode, resulting in a greater non-linear softening spring effect on the dynamics of the second mode and hence causing a larger shift in peak frequency. However, by observing $H_{11}(\omega)$ of m_1 and $H_{21}(\omega)$ of the center of the beam for m.d.o.f.1 (Figure 8), one sees that although the two responses are out of phase for effective mode 2, larger relative motion still occurs across Isolator 1 for effective mode 1. Therefore, characteristics of Isolator 1 other than amplitude-dependent stiffness may be influencing the dynamics of m.d.o.f.1. One likely possibility is that the non-linear stiffness is frequency dependent and more dominant at higher frequencies where the second peak occurs.
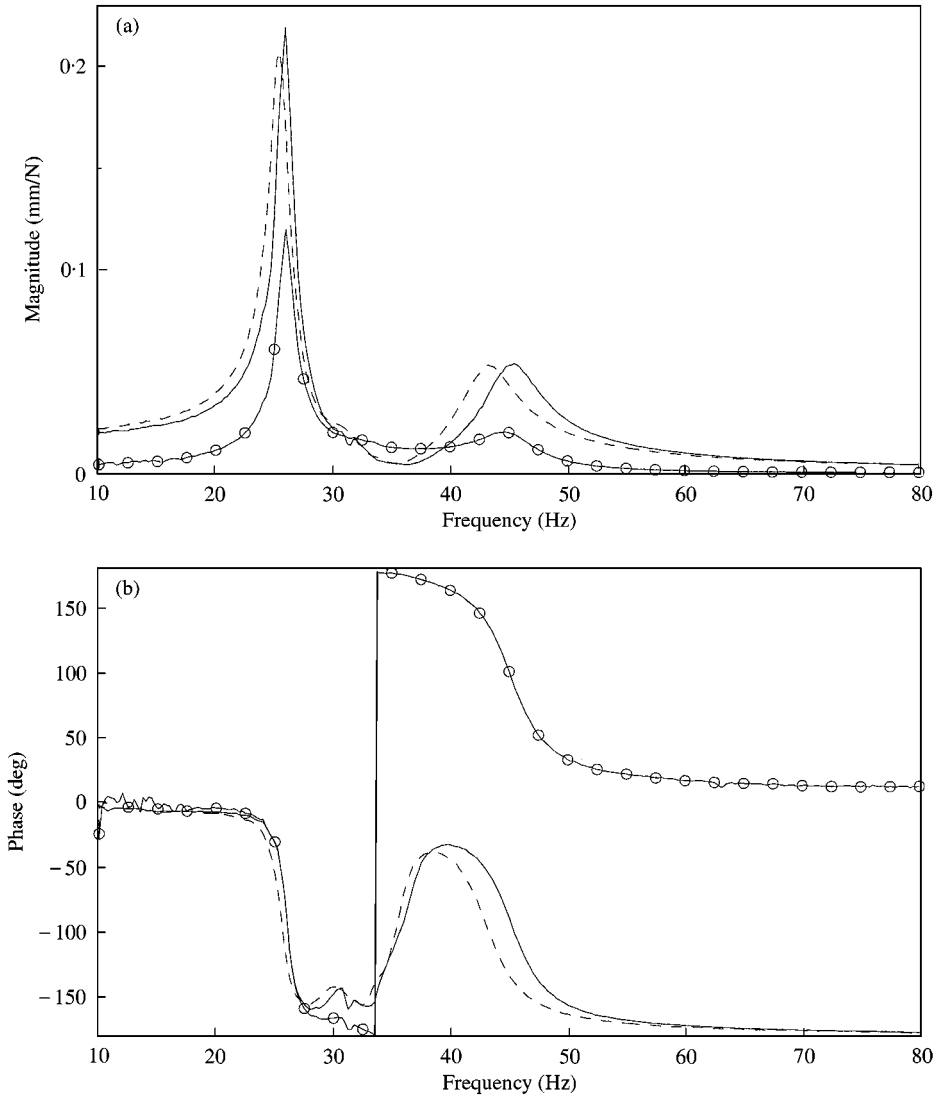
Figure 8. Measured compliance from m.d.o.f.1 configuration under random excitation: (a) magnitude; (b) phase. ——, $H_{11}(\omega)$ for lowest force level, – – – – –, $H_{11}(\omega)$ for highest force level, –O–O–, $H_{21}(\omega)$ for lowest force level.

However, this hypothesis cannot be tested with the experiments considered in this study. Instead, non-resonant dynamic stiffness experiments [3, 4] would be necessary from which one could deduce the sensitivity of the dynamic stiffness of Isolator 1 with amplitude and frequency. This will be considered for future research.

The second observation concerns the compliance spectra of Figures 8 and 10 where it can be seen that the first effective natural frequency changes more for m.d.o.f.3 than for m.d.o.f.1. This is surprising since Isolator 1 exhibits the largest change in effective stiffness in the s.d.o.f. test configuration, as given in Table 2, and hence is presumed to be the most non-linear isolator. However, observe from the compliance spectra $H_{21}(\omega)$ in Figure 10 for m.d.o.f.3 that there is very little motion of the beam. Consequently, the behavior of Isolator 3 in the m.d.o.f. configuration is similar to that in the s.d.o.f. configuration. This is
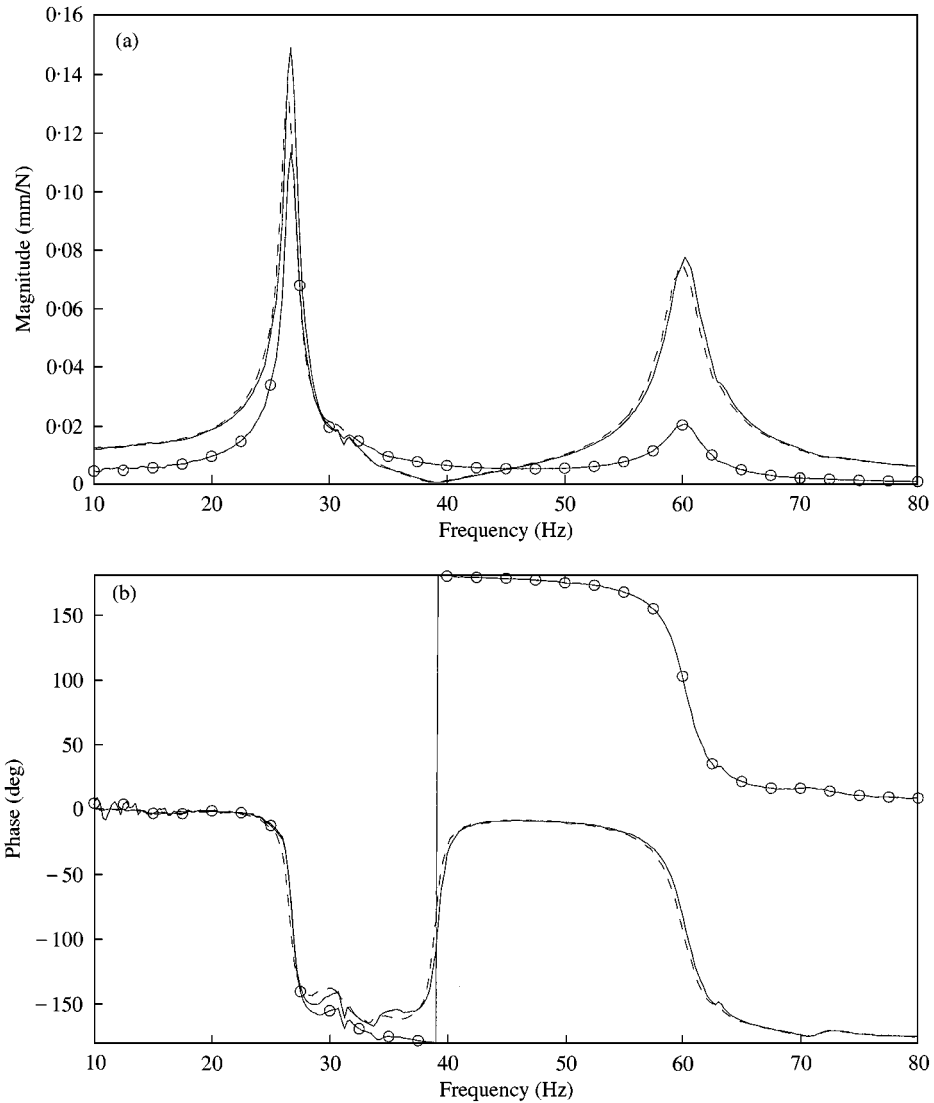
Figure 9. Measured compliance from m.d.o.f.2 configuration under random excitation: (a) magnitude; (b) phase. ——, $H_{11}(\omega)$ for lowest force level, – – – – –, $H_{11}(\omega)$ for highest force level, –O–O–, $H_{21}(\omega)$ for lowest force level.

supported by the fact that the effective natural frequencies f_n of s.d.o.f.3 (Table 2) are close in value to the effective natural frequencies f_1 of m.d.o.f.3 (Table 3). The slightly lower values for f_1 are due to the stiffness of the support beam, which is in series with the axial stiffness of the isolator. As a result of the predominate s.d.o.f. behavior of m.d.o.f.3, although the first peak of m.d.o.f.3 shifts a total of -0.8 Hz over the range of excitation levels applied, the second peak, which is not apparent on the linear amplitude scale of Figure 10, does not shift. On the other hand, for m.d.o.f.1, the first and second peaks shift -0.5 and -2.0 Hz, respectively, for a total shift of both peaks equal to -2.5 Hz over the range of excitation levels applied. Therefore, if one were to quantify the amount of non-linear stiffness of each isolator by the total amount that all of the peaks shift, Isolator 1 remains the more non-linear isolator under both the s.d.o.f. and m.d.o.f. test configurations.
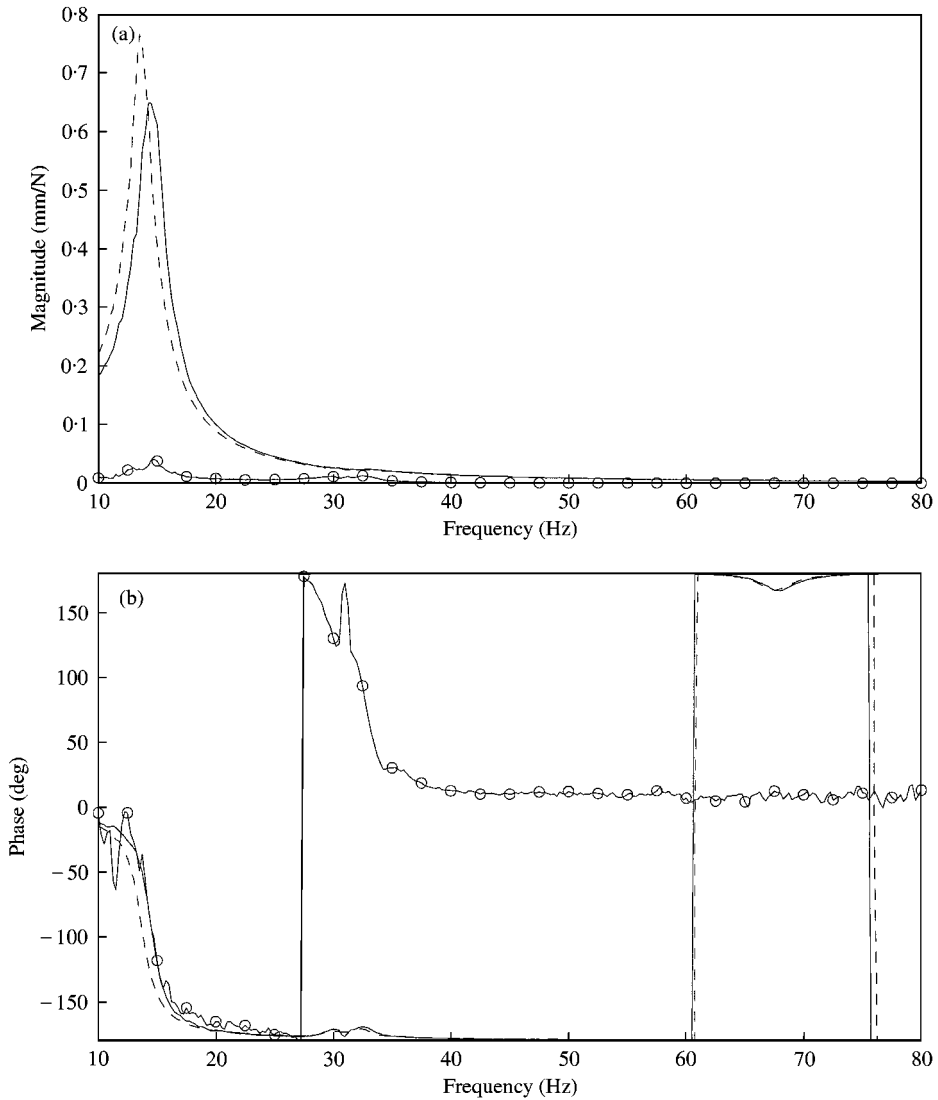
Figure 10. Measured compliance from m.d.o.f.3 configuration under random excitation: (a) magnitude; (b) phase. ——, $H_{11}(\omega)$ for lowest force level, – – – – –, $H_{11}(\omega)$ for highest force level, –O–O–, $H_{21}(\omega)$ for lowest force level.

From the second observation, one can see that the influences from the non-linear stiffness of Isolators 1 and 3 are distributed differently over each mode, i.e. the non-linear stiffness of Isolator 1 influences mode 2 more than mode 1 and the non-linear stiffness of Isolator 3 influences mode 1 and has no influence on effective mode 2. To investigate this issue further, the total amount that the first two effective natural frequencies of the m.d.o.f. configuration shift $\Delta f_1 + \Delta f_2$ as a function of excitation level is plotted in Figure 11. Also plotted is the amount that the effective natural frequencies of the s.d.o.f. configuration shift Δf_n. Interestingly, $\Delta f_1 + \Delta f_2$ and Δf_n match quite well for all three isolators. This suggests that the total influence that the non-linear stiffness has on the s.d.o.f. and m.d.o.f. system configurations is somewhat close. However, for the m.d.o.f. configuration, the influence is

TABLE 3

Effective modal parameters of m.d.o.f. configuration

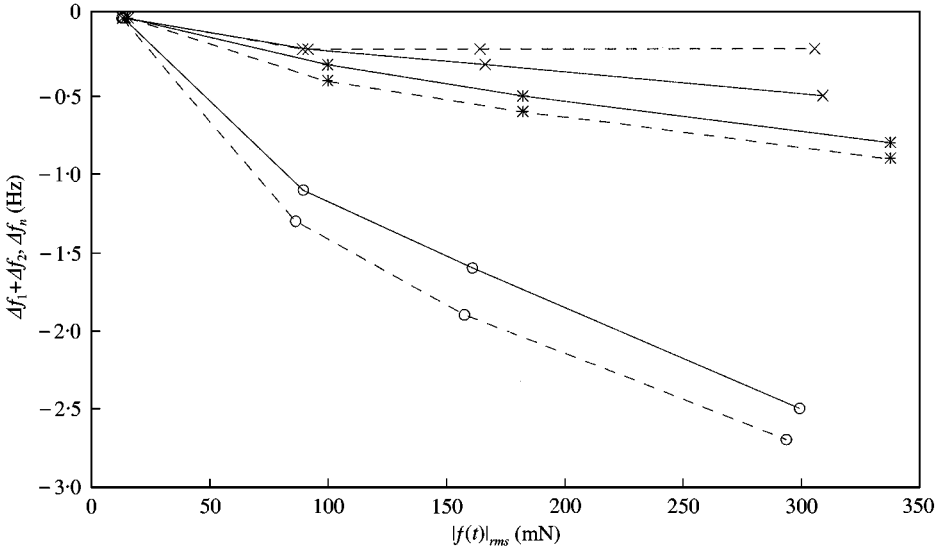| Isolator	$\|f(t)\|_{r.m.s.}$ (mN)	f_1 (Hz)	Δf_1 (Hz)	f_2 (Hz)	Δf_2 (Hz)	$\Delta f_1 + \Delta f_2$ (Hz)	ζ_1 (%)	ζ_2 (%)
	13·4	26	0	45·3	0	0	2·3	5·5
	89·5	25·8	− 0·2	44·4	− 0·9	− 1·1	2·3	5·8
1	161·1	25·7	− 0·3	44	− 1·3	− 1·6	2·5	5·9
	299·4	25·5	− 0·5	43·3	− 2·0	− 2·5	2·7	5·9
	14·2	26·8	0	60·2	0	0	1·8	2·5
	91·6	26·7	− 0·1	60·1	− 0·1	− 0·2	1·8	2·6
2	166·5	26·7	− 0·1	60	− 0·2	− 0·3	1·9	2·6
	309·3	26·6	− 0·2	59·9	− 0·3	− 0·5	2·1	2·6
	15·3	14·5	0	31	0	0	6·5	—
	99·9	14·2	− 0·3	31	0	− 0·3	6·7	—
3	182·4	14	− 0·5	31	0	− 0·5	6·8	—
	337·8	13·7	− 0·8	31	0	− 0·8	7·0	—

Figure 11. Measured changes in effective natural frequencies for s.d.o.f. and m.d.o.f. configurations. --○--, Δf_n for s.d.o.f.1; —○—, $\Delta f_1 + \Delta f_2$ for m.d.o.f.1; -- × --, Δf_n for s.d.o.f.2; — × —, $\Delta f_1 + \Delta f_2$ for m.d.o.f.2; --*--, Δf_n for s.d.o.f.3; —*—, $\Delta f_1 + \Delta f_2$ for m.d.o.f.3.

distributed over two or more modes instead of just one mode, as is the case in the s.d.o.f. configuration. In addition, note that this distribution is not necessarily the same for each isolator. This highlights the importance of "*in-situ*" m.d.o.f. testing, although the s.d.o.f. test configuration reveals the total influence that the non-linear stiffness of the isolators has on the m.d.o.f. test configuration; how each individual mode is influenced by each isolator cannot necessarily be determined from the s.d.o.f. test configuration.

The third and final observation from the m.d.o.f. configuration excited by random excitation concerns the m.d.o.f.2 compliance functions illustrated in Figure 9. Notice that
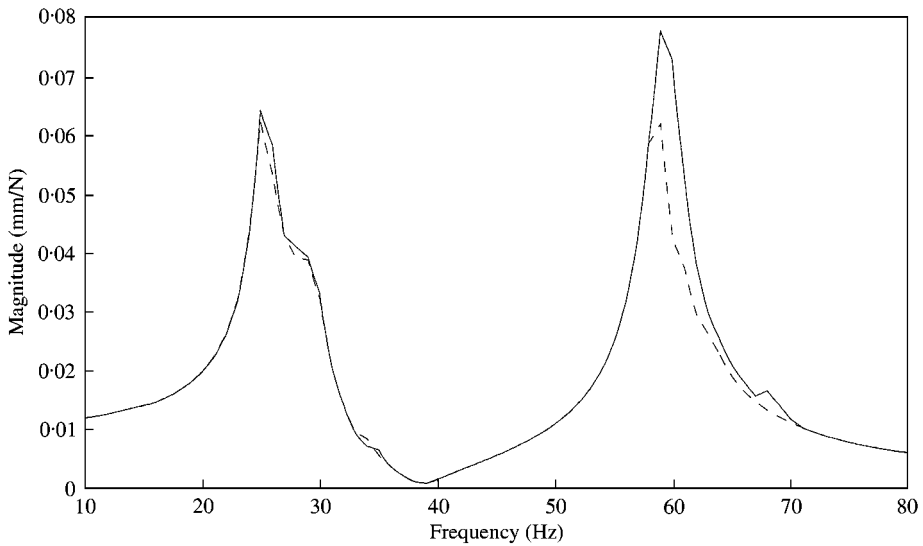
Figure 12. Measured compliance from m.d.o.f.2 configuration using swept-sine excitation. ——, positive sweep rate, – – – –, negative sweep rate.

the relative displacement across Isolator 2 is greater for effective mode 2 when m_1 is out of phase with the center of the beam, than for effective mode 1 when m_1 is in phase with the center of the beam. This is in contrast to what was seen for m.d.o.f.1. Although this contrasting phenomenon between Isolators 1 and 2 is not necessarily a result of the non-linear characteristics of the isolators, nonetheless, it also highlights the importance of "*in-situ*" m.d.o.f. testing, since it is often important to know how much isolators displace at different frequencies for design purposes such as determining clearances between components of a system [15].

Next, swept-sine excitation is applied to m_1. As with the s.d.o.f. configuration, positive and negative sweep rates are applied between 5 and 105 Hz in 1 Hz steps. Results for Isolators 1 and 3 are not illustrated since compliance functions from the positive and negative sweep rates are similar. However, illustrated in Figure 12 are compliance functions for Isolator 2. Unlike the results from the s.d.o.f. configuration, differences exist in the compliance functions from the positive and negative sweep rates. This is especially apparent in the second peak indicating strong non-linear behavior from this isolator. Also notice by comparing the first peaks from the swept-sine (Figure 12) and random (Figure 9) excitations that a 50% discrepancy in peak amplitude exists. This is possibly a result of a large increase in damping under swept-sine excitation and m.d.o.f. configuration for this isolator. These observations illustrate that excitation type influences the dynamic characteristics of the isolator since non-linear behavior is not observed for Isolator 2 under random excitation. Evidently, system configuration, i.e., s.d.o.f. versus m.d.o.f., enhances the non-linear behavior of this isolator under swept-sine excitation since this behavior is not seen for s.d.o.f.2. Note that jump phenomenon [25, 31] is not observed. This is likely a result of the high damping of the isolator [31].

Finally, sinusoidal excitations at fixed frequencies are applied to m_1. However, as observed with the s.d.o.f. configuration experiment, super-harmonics present are found to be insignificant and hence it is concluded that all three isolators behave linearly under this type of excitation in both the s.d.o.f. and m.d.o.f. test configurations.

6. QUASI-LINEAR MODELS USING CONTINUOUS SYSTEM THEORY

The initial model for predicting the dynamic behavior of the m.d.o.f. configurations is a quasi-linear model developed from the continuous system model formulated in section 2. Fixed boundary conditions are chosen to describe the clamped connections of the ends of the beam to the rigid supports of the m.d.o.f. configuration illustrated in Figure 1(b). Therefore, for the continuous model of equation 2(a, b):

$$\phi_1(0) = 0, \quad \phi_2(L) = 0, \quad \phi_{1x}(0) = 0, \quad \phi_{2x}(L) = 0. \tag{5a–d}$$

For the conditions at $x = 0.5L$, continuity and slope of the beam, shear force and moment on the beam and the equation of motion of m_1 must be satisfied:

$$\phi_1(L/2) = \phi_2(L/2), \quad \phi_{1x}(L/2) = \phi_{2x}(L/2),$$

$$EI(\phi_{1xxx}(L/2) - \phi_{2xxx}(L/2)) + k_d(\Phi - \phi_1(L/2)) + \omega^2 m_2 \phi_1(L/2) = 0,$$

$$EI(\phi_{1xx}(L/2) - \phi_{2xx}(L/2)) - \omega^2 I_2 \phi_{1x}(L/2) = 0,$$

$$- \omega^2 m_1 V + k_d(\Phi - \phi_1(L/2)) = 0, \tag{6a–e}$$

where the mass moment of inertia of m_2 is $I_2 = \frac{1}{12} m_2(3r_2^2 + h_2^2) + m_2(h_2/2)^2 = \frac{1}{12} m_2(3r_2^2 + 4h_2^2)$. These conditions are applied to equation (2a, b) to determine natural frequencies and eigenfunctions. The value used for the isolator stiffness k_d is calculated from the effective dynamic stiffness coefficient estimated from the s.d.o.f. configuration, Table 2. By conducting a parametric study at the lowest excitation level, the percentage errors ε_1 and ε_2 between the analytically predicted and experimentally measured effective natural frequencies are first minimized. The resulting parameters to model the beam are chosen different from the physical parameters of the beam in order to match the experimental natural frequencies that are lower than predicted when the physical parameters are used in the quasi-linear model. This is possibly due to compliance in the physical boundary conditions of the beam that are modelled as fixed boundary conditions by equations (4a–d). A more accurate model may result from a distribution of springs and masses to describe such clamping conditions [32]. Using the beam parameters that reduce ε_1 and ε_2, the accuracy of the quasi-linear model is next investigated at the higher excitation levels for the three isolators. Note that k_d will change as a function of isolator and excitation level.

Figure 13(a and b) illustrates changes in effective natural frequencies Δf_1 and Δf_2 predicted by the quasi-linear model as a function of excitation level along with the changes in the experimentally determined effective natural frequencies. Changes in effective natural frequencies predicted by the non-linear model, also plotted in Figure 13(a and b), are discussed in section 7. Note that slight differences exist between the excitation levels for the s.d.o.f. and m.d.o.f. configurations. Therefore, the effective natural frequencies predicted by the quasi-linear model are plotted versus the s.d.o.f. excitation levels since the values of k_d used in the quasi-linear model are determined from the s.d.o.f. configuration experiment at these levels of excitation. Although the model predicts the experimental trends for Isolator 2, results are not shown since the changes are rather small. Overall, the continuous model captures the trends of the m.d.o.f.1 and m.d.o.f.3 experimental configurations over the random excitation levels considered. Recall section 5 where it is observed how the non-linear behavior of Isolator 3 changes the first peak more than the second peak and that the opposite is true for Isolator 1. This phenomenon is predicted by the quasi-linear model as illustrated in Figure 13(a and b). Therefore, such a model may be utilized for design and performance purposes when it is desired to predict how an isolator shifts the peaks of the
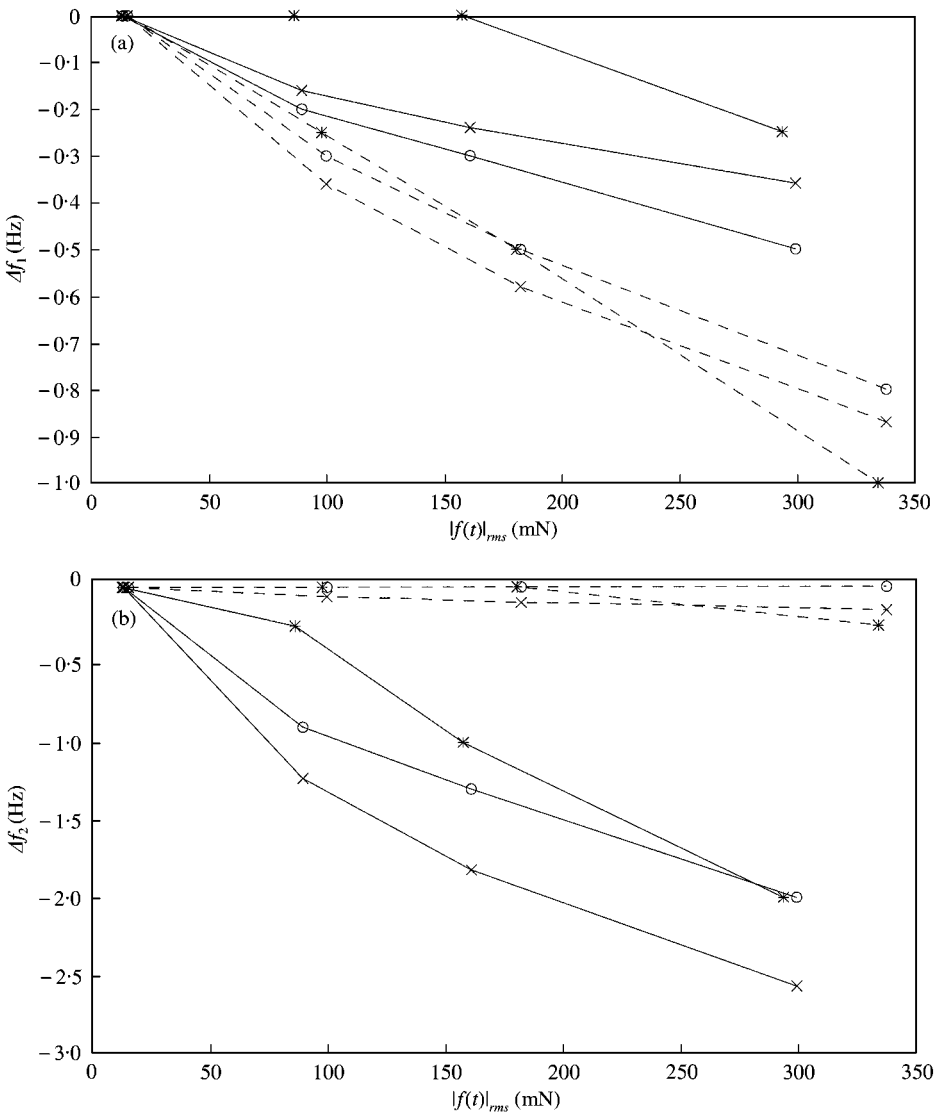
Figure 13. Measured and predicted changes in effective natural frequencies; (a) Δf_1; (b) Δf_2. —○—, measured Δf_i from m.d.o.f.1; —×—, predicted Δf_i from quasi-linear model of m.d.o.f.1; —*—, predicted Δf_i from non-linear model of m.d.o.f.1; --○--, measured Δf_i from m.d.o.f.3; $-\bar{\times}-$, predicted Δf_i from quasi-linear model of m.d.o.f.3; $-\bar{*}-$, predicted Δf_i from non-linear model of m.d.o.f.3.

m.d.o.f. configuration as a function of excitation level. However, as illustrated by the experimental characterization of section 5, the isolators respond differently to each type of excitation. Consequently, this modelling technique may lead to inaccurate forced response prediction for harmonic excitations.

7. NONLINEAR DISCRETE SYSTEM MODELS

The quasi-linear model of section 6 has been shown to capture the trends of how the natural frequencies of the m.d.o.f. configuration change with excitation level. However, the

generation of parametric "look-up" tables is necessary and the values determined for these tables are only valid at a fixed level of excitation. Therefore, only a limited amount of analysis can be conducted using such models, and in particular, these models are insufficient for transient analysis. Therefore, a single analytical model is often preferred that accurately predicts the dynamic behavior of the m.d.o.f. configuration over the excitation range considered.

To predict the amplitude-dependent response of the m.d.o.f. configuration by a single analytical model, non-linear functions are used for describing the elastic forces of the isolators. Also, the continuous system model given by equation (1a, b) is replaced by a lumped parameter model that is derived as follows. First, the beam alone is modelled with finite elements [33] and mass and stiffness matrices are realized. Second, a damping matrix is determined by assuming proportional damping for the beam. Third, the mass matrix is updated to include m_1 and m_2 and the stiffness matrix is updated to include the linear stiffness coefficient k_d of the isolator. Since non-linear damping is not considered in this study, an averaged damping coefficient is calculated for each isolator from the values given in Table 2. Finally, define the following set of coupled equations of motion:

$$\mathbf{M}_L\ddot{\mathbf{x}}(t) + \mathbf{C}_L\dot{\mathbf{x}}(t) + \mathbf{K}_L\mathbf{x}(t) + \sum_{j=1}^{n} \mathbf{a}_j y_j(t) = \mathbf{f}(t), \tag{7}$$

where $\mathbf{M}_L$, $\mathbf{C}_L$ and $\mathbf{K}_L$ are the linear mass, viscous damping and stiffness matrices of the proposed lumped model, respectively, $\mathbf{x}(t)$ is the generalized response vector and $\mathbf{f}(t)$ is the generalized force vector. Note that $\mathbf{M}_L$ is non-diagonal (but symmetric) since rotational degrees of freedom of the beam are included. The summation consists of non-linear functions $y_j(t)$ for describing the isolator's restoring force and $\mathbf{a}_j$ are vectors containing the coefficients of these functions. Note that the linear component of each isolator's elastic force is included in $\mathbf{K}_L$; therefore, the summation consists only of non-linear functions. See references [16, 17] for examples.

A fifth order Runge–Kutta–Fehlberg numerical integration routine [34] is used to simulate the response of the discrete non-linear system. Time steps Δt are held constant so that the Fourier transform can be applied to the data. For the routine to remain stable, all of the model's effective natural frequencies must lie below the Nyquist frequency f_N of the simulation, i.e., $f_{max} < f_N = 1/(2\,\Delta t)$, where f_{max} is the highest effective natural frequency of the discrete non-linear model. Unfortunately, the natural frequencies of the beam's rotational degrees of freedom can be large, requiring a very small Δt for stable simulation. This results in a large amount of computation in order to gain good spectral resolution since $\Delta f_s = 1/T = 1/(N_{dp}\,\Delta t)$, where Δf_s is the spectral resolution and N_{dp} is the number of time points calculated. Increasing the amount of computation is the total number of degrees of freedom $N_T = 2(N_{be} - 1) + 1$, where N_{be} is the number of beam elements and the $+1$ outside of the parentheses accounts for m_1. As shown below, in order to accurately represent the experimental system, choose $N_{be} \geqslant 4$ and $N_T \geqslant 7$. Therefore, large N_{dp} must be calculated for 7 degrees of freedom in order to gain good frequency resolution and an accurate model.

To alleviate this computational challenge, co-ordinate reduction is applied to the finite element beam model where the symmetric, non-diagonal mass matrix $\mathbf{M}_L$ is replaced by a diagonal lumped mass matrix $[\mathbf{M}_L^{cr}]$ [33]. The new model eliminates rotational degrees of freedom and reduces the amount of computation in two respects. First, the large natural frequencies resulting from the rotational degrees of freedom no longer exist so the restriction on small Δt can be relaxed. Second, the number of degrees of freedom reduces to $N_T = (N_{be} - 1) + 1$. Unfortunately, this solution does have one drawback. Without

rotational degrees of freedom, the mass moment of inertia I_2 cannot be included in the model. Therefore, the third effective natural frequency of the model will be greater than that of the experimental system. However, recall that since the mounting location is at $a = 0.5L$, the isolator does not influence the third mode. Therefore, analysis of the third effective mode is not included for this study.

The next step in constructing the non-linear lumped parameter model is to determine the minimum number of degrees of freedom necessary to accurately represent the experimental system. Using the same parameters for the beam as were used for the quasi-linear model and setting $\sum_{j=1}^{n} \mathbf{a}_j y_j(t) = 0$ in equation (7), natural frequencies of the discrete linear system model are determined for different values of N_{be}. For the isolator's linear stiffness coefficient, the stiffness value determined from the s.d.o.f. experimental configuration at the lowest excitation level is chosen; Table 2. This is a reasonable assumption for the value of the linear stiffness coefficient since at the lowest excitation level the isolators' response is approximately linear. For $N_{be} = 4$, the percentage error between predicted natural frequencies and measured effective natural frequencies at the lowest excitation level was found to be sufficiently small.

Now that an underlying linear model has been developed, the functions $y_j(t)$ and their respective coefficient vectors $\mathbf{a}_j$ are included to describe the non-linear stiffness behavior of the isolators. For this study, a two-term non-linear function is proposed to describe the elastic force of each isolator:

$$f^e(\Delta x_{12}(t)) = k_d \, \Delta x_{12}(t) - \gamma \, \Delta x_{12}(t) |\Delta x_{12}(t)|^{\alpha - 1}, \tag{8}$$

where $\Delta x_{12}(t)$ is the relative displacement across the isolator and α can attain non-integer values. Therefore, the summation in equation (7) reduces to a single term with $y_1(t) = \Delta x_{12}(t)|\Delta x_{12}(t)|^{\alpha - 1}$ and $\mathbf{a}_1 = [-\gamma \; \gamma \; 0 \; 0]^T$. Similar models have been analytically studied to determine transmissibility performance characteristics of non-linear isolators in s.d.o.f. configuration though non-linear damping was also included [12]. To determine optimum values, defined here as α' and γ', that result in an accurate description of each isolator under m.d.o.f. configuration, the following procedure is proposed. First, initial values α_0 and γ_0 are chosen and used in equation (8). Second, the excitation $f_1(t)$ on m_1 of the non-linear model is set equal to the measured $f_1(t)$ from the m.d.o.f. experimental configuration with the highest r.m.s. level. Therefore, the model is simulated using the same input measured from the experimental system. Third, numerical simulation is conducted to determine the response of the system. Finally, dynamic compliance functions are calculated from the simulated data and are compared with measured spectra. Different values of α and γ are then chosen and the procedure is repeated until comparison between the compliance functions is satisfactory. This initial procedure ensures that the non-linear term of equation (8) is strong enough to shift the peak frequencies the same amount as was found from experiment.

It is important to note that for a fixed value of α, there exists a limit to the largest absolute value $|\gamma|_m$ that γ can attain for the numerical simulation to remain stable. This results from the fact that since the isolators exhibit softening behavior, i.e., the peaks shift down in frequency with increasing excitation level, the second term in equation (8) is negative. Consequently, equation (8) is multi-valued, i.e., for a fixed elastic force, more than one value exists for the displacement of the isolator. A curve such as this is physically possible if some kind of breakdown occurs in the rubber composition, similar to plastic deformation, or if buckling of the isolator were to occur [6, 15]. However, when this occurs unstable numerical simulation results. Therefore, for this modelling process to be successful, equation (8) must remain single-valued over the displacement range experienced during numerical simulation. Therefore, $|\gamma|_m$ dictates whether a certain type of non-linearity given

by a fixed value of α can be used to describe each isolator. An analytical study of isolators with cubic non-linear stiffness ($\alpha = 3$) excited by random excitation has determined the maximum of the ratio $\varepsilon = \gamma/k_d$ that might prevent instability [15]. However, since values of α other than 3 are investigated for this modelling process, the analysis conducted in reference [15] is not utilized. Instead, the following procedure is used. If the analytically predicted change in effective natural frequencies is less than the experimentally measured change in effective natural frequencies for a given value of α and $\gamma = |\gamma|_m$, then this non-linearity is not strong enough to shift the effective modes of the model. Therefore, a stronger non-linearity, i.e., different value for α, is necessary. Now, one might expect that an increase in α results in a stronger non-linearity. However, for the experiments conducted here, $|\Delta x_{12}(t)| < 1$, therefore $|\Delta x_{12}(t)|^{\alpha_2} < |\Delta x_{12}(t)|^{\alpha_1}$ for $\alpha_2 > \alpha_1$. As a result, when a stronger non-linearity is necessary, α is reduced.

Once optimum values α' and γ' are determined from the above procedure, the steps described above are repeated using the measured $f_1(t)$ from the m.d.o.f. configuration with the lowest r.m.s. level. This ensures that the non-linear term is insignificant at the low excitation level since the system is assumed linear at this excitation level. If this is not the case, different values for α and γ are chosen and the procedure restarts. If the analytical and measured compliance functions for the lowest level of excitation do match well, the procedure is repeated using the intermediate r.m.s. levels. This final step determines how well the model interpolates between the two extreme levels of excitation investigated for this study.

Analysis of Isolator 2 is again not considered since the amount of elastic non-linearity exhibited by the isolator under random excitations is negligible and therefore a linear model would be sufficient. For Isolators 1 and 3, the above procedure is carried out and optimum values α' and γ' were determined to be $\alpha'_1 = 2$ and $\gamma'_1 = 50$ MN/m^2 for Isolator 1, and $\alpha'_3 = 2$ and $\gamma'_3 = 6.5$ MN/m^2 for Isolator 3. Notice that the same type of non-linearity was found optimum for describing the two isolators, i.e., $\alpha'_1 = \alpha'_3 = 2$. Also notice that $\gamma_1 > \gamma_3$. This is expected since Isolator 1 was found to be the most non-linear in stiffness of the three isolators. Changes in the effective natural frequencies for these models are plotted against measured values in Figure 13. As seen, the models predict the changes found experimentally though some deviation exists at intermediate excitation levels for m.d.o.f.1. Also, notice that both models predict the phenomenon observed in section 5, i.e., Isolator 3 shifts peak 1 more than Isolator 1 while peak 2 is unaffected, while Isolator 1 shifts peak 2 more than peak 1. This is interesting since the isolators are only represented by constant coefficient equations describing non-linear elastic and linear viscous forces. There are no parameters in the models that explicitly indicate why this phenomenon occurs. Therefore, this issue will be analytically examined in a future article.

8. CONCLUSION

The essential contributions of the study are that key non-linear stiffness characterization issues of rubber isolators are clarified, and a process is proposed that includes experiments in single and multi-degree-of-freedom configurations while different types of excitations are applied. Consequently, the following important characteristics, via experimental and analytical studies of three isolators, emerge that might not have been disclosed in traditional non-resonant testing methods [3, 4]. First, it is shown that although a general trend exists between rubber durometer and the dynamic-to-static stiffness ratio β, the non-linear elastic behavior of isolators might result in deviations from this trend, as seen with Isolator 1. Complex geometry may also significantly influence β, as seen with Isolator 3. Second,

whether isolator behavior is linear or non-linear in nature is found to depend on the type of excitation applied. Random excitation reveals non-linear behavior for Isolators 1 and 3 under both s.d.o.f. and m.d.o.f. configurations, though linear behavior is found from swept-sine and fixed-sine excitations for these two isolators. For Isolator 2, linear behavior is observed under random and fixed-sine excitations under s.d.o.f. and m.d.o.f. configuration. However, non-linear behavior is revealed under the m.d.o.f. configuration by swept-sine excitation, though linear behavior is observed for the s.d.o.f. configuration swept-sine case. Third, correlation between the non-linear behavior in s.d.o.f. and m.d.o.f. configurations is studied by comparing the changes in effective natural frequencies with excitation level. A similar trend is found for all three isolators when comparing the s.d.o.f. and m.d.o.f. configurations. However, the manner in which the influence is distributed over the effective modes of the m.d.o.f. configuration differs for each isolator, as observed with Isolators 1 and 3.

Each rubber isolator is modelled in the m.d.o.f. configuration by constructing two analytical models: a continuous quasi-linear and a discrete non-linear model. Isolator properties measured from the s.d.o.f. configuration experiment are then used to predict non-linear behavior under m.d.o.f. configuration in the continuous quasi-linear model. Changes in effective natural frequencies predicted from this model compare well with measured changes in effective natural frequencies from the m.d.o.f. experiment. For the discrete non-linear model, a non-linear stiffness term is included to capture the amplitude-dependent non-linear stiffness behavior of each isolator in the m.d.o.f. configuration. A procedure which involved numerical simulation of the discrete non-linear system is executed to determine optimum parameters for the model that reduce error between theory and experiment. Overall, this model successfully predicts changes in natural frequencies. Although the discrete non-linear model is successful, parameters of this model are obtained by using "trial-and-error"-type methods. More systematic identification techniques, such as those discussed in references [16, 17], are desirable since they are capable of estimating non-linear system parameters directly from experimental data. However, the characterization studies conducted here form an essential first step for the identification techniques that are improved by *a priori* knowledge of the types of non-linearities present [16]. This work, on the study of three rubber isolators, will serve as the basis for a future article on non-linear system identification.

REFERENCES

1. C. M. HARRIS 1996 *Shock and Vibration Handbook*. New York: McGraw-Hill; third edition.
2. P. W. ALLEN, P. B. LINDLEY and A. R. PAYNE 1967 *Use of Rubber in Engineering*. London: MacLaren and Sons, Ltd.
3. R. SINGH, G. KIM and P. V. RAVINDRA 1992 *Journal of Sound and Vibration* **158**, 219–243. Linear analysis of automotive hydro-mechanical mount with emphasis on decoupler characteristics.
4. S. NADEAU and Y. CHAMPOUX 2000 *Experimental Techniques* **24**, 21–23. Application of the direct complex stiffness method to engine mounts.
5. D. H. COOPER 1959 *Transactions of the Institution of the Rubber Industry* **35**, 166–177. Method of applying the results of dynamic testing to rubber anti-vibration systems.

6. J. A. HARRIS 1988 *Rubber Chemistry and Technology* **62**, 515–528. Design principles for vibration isolation and damping with elastomers including nonlinearity.
7. A. R. PAYNE and J. R. SCOTT 1960 *Engineering Design with Rubber*. New York: Interscience Publishers, Inc.
8. R. G. DEJONG, G. E. ERMER, C. S. PAYDENKAR and T. M. REMTEMA 1998 *Proceedings of Noise-Con '98*, 383–390. High frequency dynamic properties of rubber isolation elements.
9. T. P. CALDWELL 1998 *Proceedings of Noise-Con '98*, 371–376. Improved modeling procedure for predicting airplane stowage bin isolator performance.
10. B. P. BYAM and C. J. RADCLIFFE 1997 *Proceedings of the ASME Dynamic Systems and Controls Division* **61**, 751–756. Statistical energy analysis model and connectors for automotive vibration isolation mounts.
11. W. L. LI and P. LAVRICH 1998 *Proceedings of Noise-Con '98*, 377–382. Determination of power flows through vibration isolators.
12. B. RAVINDRA and A. K. MALLIK 1994 *Journal of Sound and Vibration* **170**, 325–337. Performance of non-linear vibration isolators under harmonic excitation.
13. N. CHANDRA SHEKHAR, H. HATWAL and A. K. MALLIK 1999 *Journal of Sound and Vibration* **214**, 589–603. Response of non-linear dissipative shock isolators.
14. N. CHANDRA SHEKHAR, H. HATWAL and A. K. MALLIK 1999 *Journal of Sound and Vibration* **227**, 293–307. Performance of non-linear isolators and absorbers to shock excitation.
15. C. L. KIRK 1988 *Journal of Sound and Vibration* **124**, 157–182. Non-linear random vibration isolators.
16. C. M. RICHARDS and R. SINGH 1999 *Journal of Sound and Vibration* **220**, 413–450. Feasibility of identifying nonlinear vibratory systems consisting of unknown polynomial forms.
17. C. M. RICHARDS and R. SINGH 1998 *Journal of Sound and Vibration* **213**, 673–708. Identification of multi-degree-of-freedom non-linear systems under random excitations by the "reverse path" spectral method.
18. A. K. MALLIK, V. KHER, M. PURI and H. HATWAL 1999 *Journal of Sound and Vibration* **219**, 239–253. On the modelling of non-linear elastomeric vibration isolators.
19. Y. Q. NI, J. M. KO and C. W. WONG 1997 *Journal of Sound and Vibration* **217**, 737–756. Identification of non-linear hysteretic isolators from periodic vibration tests.
20. Y.-K. WEN 1976 *Proceedings of ASCE, Journal of the Engineering Mechanics Division* **102**, 249–263. Method for random vibration of hysteretic systems.
21. M. BERG 1998 *Vehicle System Dynamics* **30**, 197–212. A non-linear rubber spring model for rail vehicle dynamics analysis.
22. H. STORCK and H. SUMALI 1999 *SAE, International Off-Highway and Powerplant Congress and Exposition, Indianapolis*. Characterization of a vibration damping mount.
23. C. M. RICHARDS and R. SINGH 1998 *Proceedings of Noise-Con'98*, 391–396. Identification of nonlinear properties of rubber isolators using experimental and analytical methods.
24. D. J. THOMPSON, W. J. VAN VLIET and J. W. VERHEIJ 1998 *Journal of Sound and Vibration* **213**(1), 169–188. Developments of the indirect method for measuring the high frequency dynamic stiffness of resilient elements.
25. L. MEIROVITCH 1967 *Analytical Methods in Vibrations*. London: The Macmillan Company, Collier–MacMillan Limited.
26. Tech Products Corporation 1996 *Noise and Vibration Control Products* Catalog.
27. S. C. CHAPRA and R. P. CANALE 1988 *Numerical Methods for Engineers*. New York: McGraw-Hill, Inc.
28. H. K. MILNE 1984 *Journal of Sound and Vibration* **93**, 469–471. A note on the calculation of frequency response functions by the inverse method.
29. L. D. MITCHELL 1982 *American Society of Mechanical Engineers, Journal of Mechanical Design* **104**, 277–279. Improved methods for the Fast Fourier Transform (FFT) calculation of the frequency response function.
30. GENRAD, Inc. 1994 THE STAR SYSTEM *Reference Guide*.
31. F. S. TSE, I. E. MORSE and R. T. HINKLE 1978 *Mechanical Vibrations, Theory and Applications*. Boston: Allyn and Bacon, Inc.
32. H. VINAYAK and R. SINGH 1996 *Journal of Sound and Vibration* **192**, 741–769. Eigensolutions of annular-like elastic disks with intentionally removed or added material.
33. J. N. REDDY 1993 *An Introduction to The Finite Element Method*: New York: McGraw-Hill Inc.; second edition.
34. G. E. FORSYTHE, M. A. MALCOLM and C. B. MOLER 1977 *Computer Methods for Mathematical Computation*. Englewood Cliffs, NJ: Prentice-Hall.

APPENDIX A: NOMENCLATURE

a	distance from end of beam to mounting location
$\mathbf{a}$	coefficient matrix
b	beam thickness
c	linear viscous damping coefficient
$\mathbf{C}$	damping matrix
E	modulus of elasticity
f	effective natural frequency (Hz)
Δf	change in effective natural frequency (Hz)
f_{max}	maximum frequency range of interest
Δf_s	spectral resolution
f^e	elastic force
$\mathbf{f}$	excitation vector
$f_1(t)$	excitation applied to m_1
$|f_1(t)|$	magnitude of $f_1(t)$
F	spectrum of excitation
g	dynamic elastic force of isolator
G	total dynamic force of isolator
h	static stiffness of isolator or height of cylinder m_2
H	frequency response
i	$\sqrt{-1}$
I	second moment of inertia
k	stiffness coefficient
$\mathbf{K}$	stiffness matrix
L	length of beam
m	mass
$\mathbf{M}$	mass matrix
N_{be}	number of beam elements
N_{dp}	number of calculated time points
N_T	total number of degrees of freedom
r	radius of cylinder m_2
R	coefficient of determination
r.m.s.	root mean square
t	time (s)
t_r	recording time for static stiffness experiment
u	transverse displacement of beam
w	width of beam
x	displacement
$\mathbf{x}$	displacement vector
X	spectrum of displacement
y	distance along length of beam or non-linear stiffness function
α	exponent of non-linear stiffness function
β	dynamic-to-static stiffness ratio
ε	percentage error
ϕ	displacement amplitude of beam
Φ	displacement amplitude of isolated mass m_1
γ	coefficient of non-linear stiffness function
ρ'	mass per unit length
ω	frequency (rad/s)
Ξ	static stiffness polynomial model
ζ	damping ratio

Subscripts

d	dynamic
L	linear
o	initial value
s	static
n	natural frequency

N	Nyquist frequency
r.m.s.	root mean square
x	differentiation with respect to displacement

Superscripts

| $'$ | optimum value |
| cr | co-ordinate reduction |